

Dynamic piezoelectric response of relaxor single crystal under electrically driven inter-ferroelectric phase transformations

E.A. Patterson¹, M. Staruch¹, B. Matis², S. Young³, S.E. Lofland⁴, L. Antonelli⁵, F. Blackmon⁵, D. Damjanovic⁶, M.G. Cain⁷, P.B.J. Thompson^{8,9}, C.A. Lucas^{8,9}, and P. Finkel^{1*}

¹Materials Science and Technology Division, U.S. Naval Research Laboratory, Washington DC 20375, USA

²Acoustics Division, U.S. Naval Research Laboratory, Washington DC 20375, USA

³Department of Physics and Astronomy, University of Missouri – Kansas City, Kansas City, Missouri, 64110, USA

⁴Department of Physics, Rowan University, Glassboro, NJ, 08028, USA

⁵Naval Undersea Warfare Center (NUWC), Newport, RI 02841, USA

⁶Group for Ferroelectrics and Functional Oxides, Department of Materials Science, Swiss Federal Institute of Technology, EPFL, EPFL-SCI-STI-DD; Bât. MX D236, Station 12 CH-1015 Lausanne, Switzerland

⁷Electrosiences Ltd., Farnham, Surrey, GU9 9QT, U.K.

⁸XMaS Beamline, European Synchrotron Radiation Facility, Grenoble, F-38043, France

⁹Department of Physics, University of Liverpool, Oliver Lodge Laboratory, Liverpool. L69 7ZE. U.K.

Abstract

In this work, we demonstrate that $x\text{Pb}(\text{In}_{1/2}\text{Nb}_{1/2})\text{O}_3-(1-x-y)\text{Pb}(\text{Mg}_{1/3}\text{Nb}_{2/3})\text{O}_3-y\text{PbTiO}_3$ [110]-poled domain-engineered relaxor single crystals can be dynamically and reversibly driven through a ferroelectric-ferroelectric phase transition exhibiting highly enhanced piezoelectric response in a wide range of frequencies. Realization of this phase switching requires an applied compressive stress close to the critical values for the inter-ferroelectric phase transition, which can then be induced by a relatively small electric field (≤ 0.2 kV/mm). The required critical stress was established by *in situ* stress and X-ray diffraction measurements. The effective d_{32} coefficient measured dynamically up to 70 Hz was shown to be consistently twice that of the linear piezoelectric mode measured below the phase transformation region. The crystal was installed into a prototype transducer based on a Tonpilz configuration. The performance of the transducer was tested in water and showed up to 15 dB_{SPL} higher acoustic power radiated when the crystal was driven through the phase transition than when operating in the linear piezoelectric regime.

*Corresponding author: peter.finkel@nrl.navy.mil

37 Continued development of highly efficient transducers for high-power, low-frequency,
38 compact-sized sound projectors demands a new class of materials with enhanced properties. High
39 power underwater acoustic projectors are generally very large and heavy, but recent single crystal
40 transducer development [1,2] promises significant size and weight reductions [3,4]. Specifically,
41 domain-engineered relaxor $(1-x)\text{Pb}(\text{Mg}_{1/3}\text{Nb}_{2/3}\text{O}_3-x\text{PbTiO}_3)$ (PMN-PT) and $(1-x)\text{Pb}$
42 $\text{Zn}_{1/3}\text{Nb}_{2/3}\text{O}_3-x\text{PbTiO}_3$ (PZN-PT) systems poled along the equivalent nonpolar (001)_c
43 pseudocubic direction are of highest interest. The crystals with compositions close to the
44 morphotropic phase boundary (MPB) [5–9] showed high electromechanical coupling factors ~ 0.9 ,
45 and large piezoelectric coefficients up to 2000 pm/V [3–5]. It was concluded that this phenomenon
46 of enhanced piezoelectricity can be linked to the presence of intermediate monoclinic (F_M) and
47 orthorhombic (F_O) ferroelectric states in between the ferroelectric rhombohedral (F_R) and
48 tetragonal (F_T) phases, allowing for enhanced polarization rotation [3–8]. This F_R -to- F_T phase
49 transformation can also be accessed electrically [3] with maximum strains on the order of 1% [4]
50 in binary compositions of PZN-PT, whereas large anhysteretic strains of up to 0.6% in PMN-PT
51 [5] have been reported. Electrically induced discontinuities in strain were studied by Davis *et al.*
52 [11] and were asserted to be a first-order-like phase transition.

53 In addition, an elastic instability was reported in both binary and ternary domain engineered
54 single crystals subjected to uniaxial stresses [9–12]. The isothermal elastic response with harmonic
55 stress (~ 50 MPa) of domain engineered (3-3 and 3-2 modes) PZN-PT single crystals with
56 composition near MPB was investigated by Amin and Cross [13]. Okawara and Amin [11]
57 observed a reversible and hysteretic stress-strain response of these crystals that is characterized by
58 a large and sharp strain discontinuity (up to 0.5%) occurring at a critical stress. This strain was
59 attributed to a stress-induced F_R to F_O transition caused by polarization rotation under mechanical

This is the author's peer reviewed, accepted manuscript. However, the online version of record will be different from this version once it has been copyedited and typeset.

PLEASE CITE THIS ARTICLE AS DOI: 10.1063/5.0007820

60 compression. The reversible effect is speculated to be due to internal electric fields such as those
61 associated with charged domain walls [12]. Similar observations in domain engineered ternary
62 $x\text{Pb}(\text{In}_{1/2}\text{Nb}_{1/2})\text{O}_3-(1-x-y)\text{Pb}(\text{Mg}_{1/3}\text{Nb}_{2/3})\text{O}_3-y\text{PbTiO}_3$ ($x=0.24$, $y=0.32$) (PIN-PMN-PT) single
63 crystals were reported by Finkel *et al.* [14]. Recently, using mechanically biased PIN-PMN-PT
64 (110) poled crystals we presented a method to deliver strain levels of $\sim 0.5\%$ at relatively low (\sim
65 0.1 kV/mm) drive fields, representing a fourfold increase in strain at only 20% of the drive field
66 as compared to those of other piezoelectric relaxor ferroelectric single crystals (*e.g.* PMN-PT)
67 [15,16]. Despite the critical importance for applications these phase switching phenomena in PIN-
68 PMN-PT crystals were reported predominately under quasi-static or nearly DC conditions. So far
69 there has been limited work extending this intrinsic structural phase switching phenomenon into
70 higher frequency range required for real sound generating devices. Further progress in exploiting
71 these large enhanced piezoelectric properties potentially leading to transducers with even greater
72 performance requires the study of the underlying mechanism of this phase transformation. In this
73 work, we demonstrate dynamic response based on the large electro-strain generated in the
74 crystalline phase transition found in relaxor ferroelectric [110]-oriented, domain-engineered PIN-
75 PMN-PT single crystals. To achieve this, we have applied a compressive mechanical stress close
76 to the critical compressive stress σ_c needed for phase transformation from F_R to F_O , *i.e.* mechanical
77 confinement. Compared to the field-induced strain of $\sim 0.5\%$ at 2 kV/mm in PZN-PT single
78 crystals as reported by Park *et al.* [7], the present results show similar strains but with over an
79 order of magnitude reduction in field.

80 Rectangular bars of PIN-PMN-PT with dimensions of $4 \times 4 \times 12$ mm were procured with
81 the longest edge oriented along the [001] while the other faces were oriented along the $\langle 110 \rangle$.

This is the author's peer reviewed, accepted manuscript. However, the online version of record will be different from this version once it has been copyedited and typeset.

PLEASE CITE THIS ARTICLE AS DOI: 10.1063/5.0007820

82 These bars were compressed along the [001] in several different loading devices for testing of the
83 piezoelectric coefficient d_{32} at different frequencies and compressive stresses.

84 First in order to confirm if the prestress is sufficient for reaching the required critical
85 threshold needed for realization of the transition to a phase that had been previously described as
86 orthorhombic [8, 10, 11, 13-15]. To ensure we can achieve this F_R -to- F_o phase transformation we
87 recorded the stress- strain response this time using a custom-built stress rig permitting *in situ* X-
88 ray diffraction characterization (see [Supplementary information*1](#)). Full 3D reciprocal mapping
89 with a 2D camera revealed the structural phases present as a function of stress and field (more
90 details can be found in ref. [18]). Strain was measured with a strain gauge affixed to the sample
91 on the $(\bar{1}10)$ specular face, aligned in the [001] direction. Figure 1 shows the X-ray diffraction
92 $(\bar{1}10)$ – referenced here with pseudo-cubic indices - lattice parameter change as a function of
93 applied uniaxial compressive stress at zero applied electric field along with simultaneously
94 measured strain, corrected with a Poisson ratio of 0.37 to make the two graphs match. An initial
95 quasi-linear strain softening is identified as the low stress F_R phase. At a critical stress, $\sigma_c > 20$
96 MPa the elastic properties changed dramatically to a much stiffer response, characteristic of the
97 high-stress phase F_o . The X-ray diffraction data from the (111) reflection plotted as X-ray
98 intensity (H-K) contour plots at constant L ($L=1.131$) (Figure 1, insets) show two distinct (HKL)
99 diffracting conditions at low stress transforming to only one (HKL) condition at stresses above σ_c .

100 Next, the quasi-static (< 1 Hz) stress-strain behavior of the crystals was characterized in a
101 load frame (Instron), and from this measurement the critical stress σ_c for the phase transition was
102 determined to be close to the values evaluated from the *in situ* X-ray experiment and to the values

*1 The data that supports the findings of this study are available within the article and its supplementary material.

103 reported earlier [17]. Strain and polarization hysteresis curves were measured with a ferroelectric
104 test system (Radiant Technologies) while the sample remained mechanically confined under stress
105 along the [001] direction (as shown in the insert of Figure 1a) accompanied by an electric field
106 applied along [110]. Several of the resulting strain vs. electric field curves at variable compressive
107 stress ranging from 20 to 26 MPa are shown in Figure 2. It should be noted that in this range of
108 compressive stress, an amplitude of the applied electric field < 0.2 kV/mm was sufficiently high
109 to cycle from F_R to F_O and back to F_R . This sharp jump in strain (up to 2000 microstrain) was
110 triggered reversibly with low hysteresis and approximately independent of pre-stress conditions.

111 Subsequent to this, a dynamic piezo-analyzer was used to evaluate the direct d_{32}
112 piezoelectric response under mechanical compressive load up to 50 MPa, but this time with an AC
113 stress signal (at 1 Hz and 70 Hz) applied superposed on the static preload value for three preloads
114 representing F_R (< 20 MPa), F_{TRANS} (~ 23 MPa) and F_O (> 26 MPa) phases. The dynamic charge-
115 stress relation was measured with a home-built press. The press contains a quartz reference sensor
116 to measure the force, a PZT actuator, two stiff zirconia columns with steel caps for electrical
117 contacts between which the sample is placed, and a stepper motor, all connected mechanically in
118 series and contained within a rigid steel frame. The AC stress is generated by the PZT actuator.
119 The piezoelectric charges produced by the quartz sensor and the sample are measured by two
120 separate charge amplifiers and recorded by an oscilloscope. Both longitudinal and transverse
121 piezoelectric response can be measured by appropriate orientation of the electroded faces with
122 respect to the crystallographic axes of the sample and direction along which the stress is applied.
123 For charge induced by stress during the phase transition, the compressive force was only applied
124 from 0 to 40 MPa by the stepper motor. The total duration of force application and release for this
125 technique lasts approximately 2 minutes. More details can be found in Refs. [19,20].

126 The stress-polarization dependence is plotted in Figure 3(a). It is notable that there is almost
127 no observable hysteresis upon loading and unloading. There are three clearly observable regions
128 with different slopes (as denoted by blue, red and green symbols in Fig 3(a)) which correspond to
129 the two phases separated by the sharply increasing polarization region where the transition between
130 them is occurring. As shown by d_{32} versus stress in the inset of Figure 3(a), the value is relatively
131 constant in the F_R condition with a large spike at stresses near the phase transition at ~ 20 MPa that
132 corresponds to the optimal loading condition (σ_c) for F_{TRANS} . At higher stress values, d_{32} drops
133 off significantly once the crystal is in the orthorhombic regime.

134 The crystals were also tested in a special spring and mechanical screw loaded fixture and
135 compressively stressed in the ranges as described above. At these loads, bipolar electrical field-
136 strain hysteresis measurements were performed at fields of 0.3 kV/mm at 10 Hz in order to
137 characterize the converse d_{32}^* piezoelectric coefficient (*i.e.* normalized maximum strain at the
138 maximum applied electric field). The electric field dependence of the strain is plotted in Figure
139 3(b) while the crystal is held at a pre-stress corresponding to either the F_R or F_O phases or at σ_c to
140 achieve the phase transition (F_{TRANS}). There is a clear difference in the total strain generated for
141 the same electric field swept at 10 Hz.

142 The d_{32} and d_{32}^* values as calculated from the slopes of these experiments , as well as the
143 values calculated from the dynamic d_{32} setup , are summarized in Table 1 for the three loading
144 conditions of interest corresponding to F_R , F_O and F_{TRANS} regions as denoted by blue , red and
145 green symbols in Fig 1a) From the data in Table 1 it is clear that the d_{32} and d_{32}^* values are
146 substantially higher in the transition region, although there is a fairly large variation in magnitude
147 depending on the measurement technique. The differences may be due to how the measurements

148 were done (i.e. changes in the boundary conditions in different load frames) since the dynamic d_{32}
149 measurement showed only a modest decrease as the frequency changed from 1 to 70 Hz.

150 After initial characterization of the crystal under low frequency drive conditions the crystal
151 was installed into a transducer assembly (a Tonpilz-type design) driven over broader range of
152 frequencies in tens of kHz range. For this, electrical leads were attached to the electrodes on the
153 surface of the crystal, and the crystal was inserted into the transducer apparatus as shown in the
154 schematic in Figure 4. A screw on the top was used to apply an adjustable compressive pre-load
155 to the crystal. The crystal was placed between two ceramic shims, and for optimal boundary
156 conditions there were several spring washers below the head adapter. The sound was transmitted
157 from the cone on the opposite side, which was submerged in water and directed at the hydrophone.
158 The transducer was not potted with oil or otherwise waterproofed and remained above the surface
159 of the water during testing. Initial testing with a square wave pulse was done at the Naval Undersea
160 Warfare Center in Newport, RI. Comparison tests, and then subsequently final characterization
161 discussed herein, were performed at the NRL facility described in details in [Supplementary](#)
162 [section²](#).

163 There are various resonances within the structure and those resonances shift in frequency
164 and amplitude with applied stress due to the change in sample properties as confirmed by
165 impedance measurements (Fig. 5(a)); however the general trend in the sound pressure level (SPL)
166 data is in agreement with the measured piezoelectric coefficients for the three different pre-stress
167 conditions. The SPL for a 400 V chirp pulse with broad spectrum waveform [Figure 5(b)] shows
168 an overall higher result for the crystal under F_{TRANS} loading conditions in the entire frequency
169 range, and particularly above 10 kHz. At a local maximum near 27 kHz, there is an enhancement

² The data that supports the findings of this study are available within the article and its supplementary material

170 of 15 dB in SPL between the F_{TRANS} (76 dB) and F_R (60 dB) data and a similarly large enhancement
171 as compared to when the sample is in the F_0 regime. This suggests that even at much higher
172 frequencies than shown in Table 1, the relationship between the d_{32}^* coefficients still holds and
173 that the corresponding increase in strain generated through the phase transition directly translates
174 to an increase in acoustic pressure level.

175 We also monitored temperature of the crystal inside the transducer using an IR camera
176 (FLIR E95) while driving at 500 V at 1000 Hz through the phase transition for ~ 30 min to achieve
177 equilibrium and found that the sample heating is much less than 1 °C under continuous operation.
178 With negligible heat dissipated and the lack of fatigue previously observed for tens of millions
179 cycles in these PIN-PMN-PT [14-16], we believe these results demonstrate the great potential for
180 using this phase transformational regime for high-power sound-generation transduction. With
181 further chemical and microstructural optimization of single crystal materials - specifically focused
182 on their dynamic piezoelectric properties under stress - we anticipate that such large strains can be
183 generated at even lower fields .

184 In summary, we investigated and demonstrated broadband dynamic nonlinear piezoelectric
185 response in [011] poled ferroelectric 0.24PIN-0.44PMN-0.32PT relaxor single crystals and how
186 to capture this large response for potential application in acoustic transducers. It was shown that
187 as compared to linear rhombohedral or orthorhombic modes, the effective nonlinear dynamic d_{32}
188 or d_{32}^* coefficient is almost a factor of two higher, and this enhancement persists over a wide range
189 of frequencies. Through the use of *in situ* compressive-stress X-ray diffraction the optimum
190 mechanical bias was identified as being close to the critical stress for triggering rhombohedral –
191 orthorhombic phase transformations, and we demonstrated excellent performance of a prototype
192 transducer element and the viability of exploiting this effect. The sound pressure level was

193 enhanced (10-15 dB) throughout a large frequency range when the crystal is driven through the
194 phase transition as compared to when it was in either of the linear piezoelectric regimes. The
195 advantage of implementing nonlinear phase switching that is permitted in [110]-poled PIN-PMN-
196 PT single crystals leads to opportunities to produce acoustic sources with enhanced performance
197 at lower applied fields for highly efficient sound transduction.

198

199 Supplementary Material

200 The supplemental material contains full description of a custom-built stress rig permitting
201 *in situ* X-ray diffraction characterization and also detailed apparatus and the system for in water
202 SPL tests for acoustic sensor.

203 The authors would like to acknowledge funding from the Office of Naval Research under
204 the U.S. Naval Research Laboratory's Basic Research Program, and Office of Naval Research
205 Global, ONRG - NICOP Project Number: N62909-18-1-2008 Electrosiences Ltd.. Parts of this
206 research work was carried in the framework of the ADVENT project (Grant Number: 16ENG06
207 ADVENT) which is supported by the European Metrology Programme for Innovation and
208 Research (EMPIR). The EMPIR initiative is co-funded by the European's Horizon 2020 research
209 and innovation program and the EMPIR Participating States.

210

211 All data generated or analyzed during this study are included in this published article (and its
212 supplementary information files) and also are available from the corresponding author on
213 reasonable request.

214

215

216

This is the author's peer reviewed, accepted manuscript. However, the online version of record will be different from this version once it has been copyedited and typeset.

PLEASE CITE THIS ARTICLE AS DOI: 10.1063/5.0007820

217
218
219
220
221
222

223
224
225
226
227
228
229
230
231
232
233
234
235
236
237
238
239
240

Table 1: Values of d_{32}^* and d_{32} derived from bipolar electric field – strain hysteresis (10 Hz, **a** – **E-S Hyst.**), slopes of stress-polarization (20 mHz, **b.**), and from dynamic d_{32} measurements (1 and 70 Hz, **c.**).

	F_R	F_{TRANS}	F_O	Setup
20 mHz	1690 pC/N	3440 pC/N	184 pC/N	b
1 Hz	1200 pC/N	1700 pC/N	222 pC/N	c
10 Hz	824 pm/V	2090 pm/V	98.0 pm/V	a
70 Hz	1310 pC/N	1570 pC/N	209 pC/N	c

This is the author's peer reviewed, accepted manuscript. However, the online version of record will be different from this version once it has been copyedited and typeset.

PLEASE CITE THIS ARTICLE AS DOI: 10.1063/5.0007820

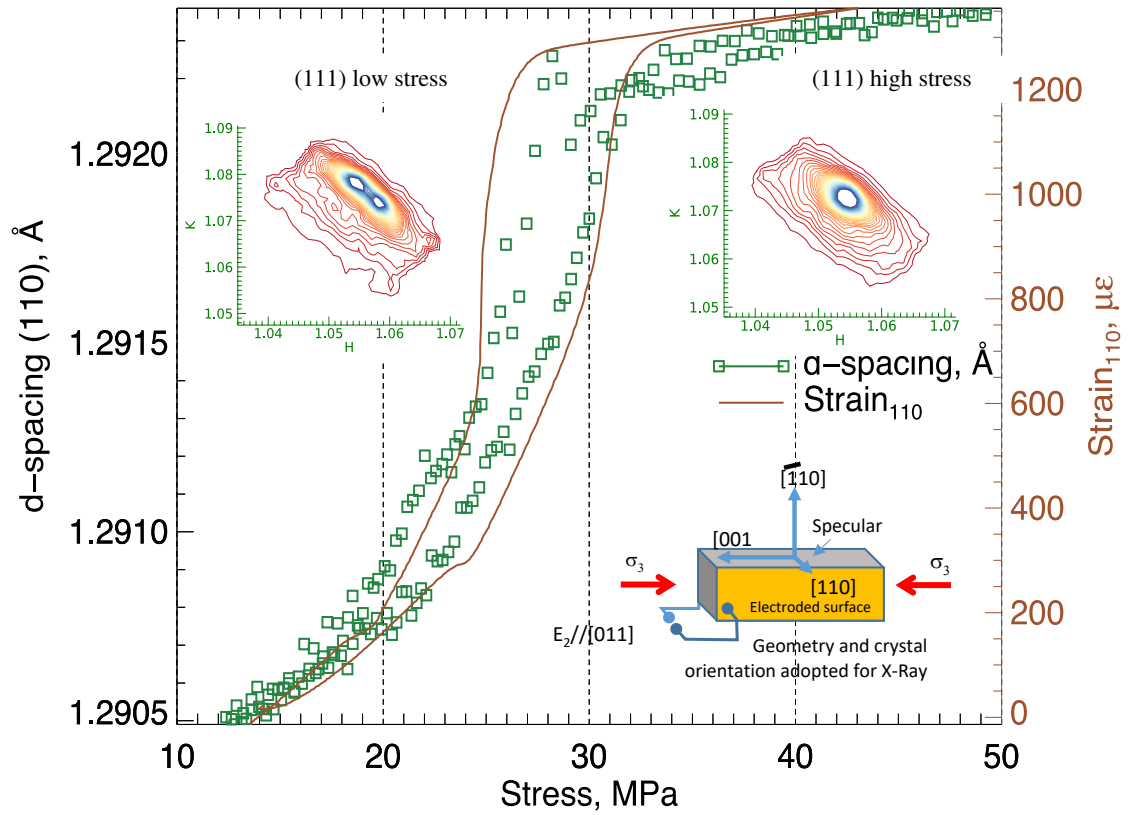


Figure 1. *In situ* X-ray diffraction of the $(\bar{1}10)c$ reflection (d-spacing - green squares, and all reflection indices based on a pseudo cubic unit cell) compared to macroscopic strain (solid line) measured as a function of applied uniaxial stress at zero applied field. There is a stress-induced transformation from two phases/domains at low stress to one single (higher modulus) phase at high stresses. The features present in the diffraction data are real and repeatable and indicate pathways from low stress rhombohedral symmetry to a higher stress lower symmetry phase. Contour maps show the $(111)c$ diffraction contrast for low stress (10 MPa), and highest stress states (48 MPa), and the sample X-ray configuration schematic is provided for orientation clarity. Macroscopic strain is recorded along $(001)c$ and a Poisson ratio of 0.37 is used to match to the X-ray data.

This is the author's peer reviewed, accepted manuscript. However, the online version of record will be different from this version once it has been copyedited and typeset.

PLEASE CITE THIS ARTICLE AS DOI: 10.1063/5.0007820

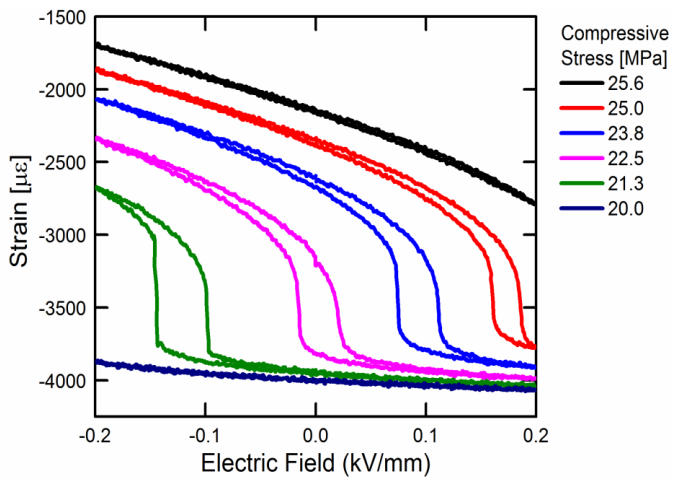


Figure 2 Strain measured quasi-statically at 1 Hz depicting large nonlinearity due to the F_R to F_0 phase transition at various stresses from 20-26 MPa.

This is the author's peer reviewed, accepted manuscript. However, the online version of record will be different from this version once it has been copyedited and typeset.

PLEASE CITE THIS ARTICLE AS DOI: 10.1063/5.0007820

265
266

267
268
269
270
271
272
273
274

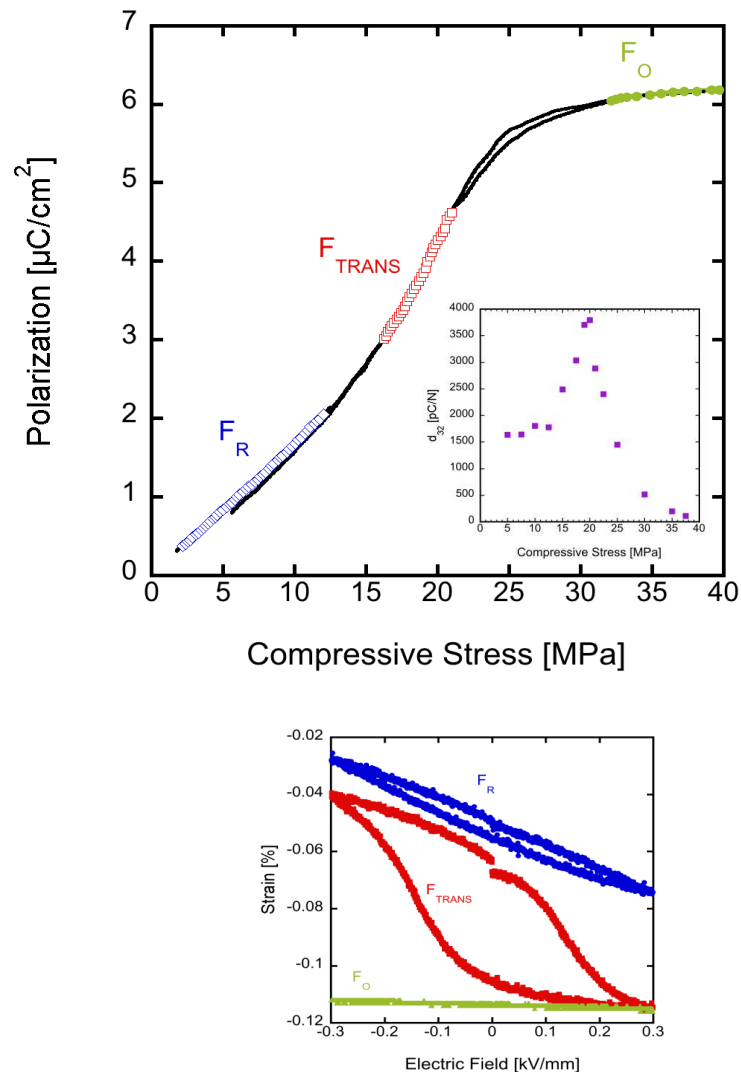
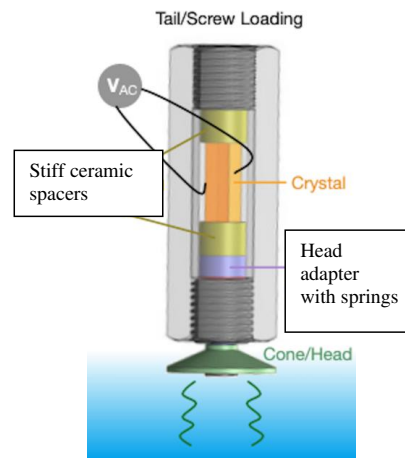


Figure 3. (a) Stress dependence of the polarization at 20 mHz with slopes used for d_{32} highlighted at the three regions of interest F_R , F_{TRANS} , and F_O denoted by blue, red and green symbols respectively that was also used to calculate the slope for d_{32} values reported in the Table 1. Inset shows d_{32} vs. stress as calculated from the slope. (b) Strain as a function of electric field measured at 10 Hz for three corresponding regions (F_R , F_{TRANS} , and F_O) as above.

This is the author's peer reviewed, accepted manuscript. However, the online version of record will be different from this version once it has been copyedited and typeset.

PLEASE CITE THIS ARTICLE AS DOI: 10.1063/5.0007820

275
276

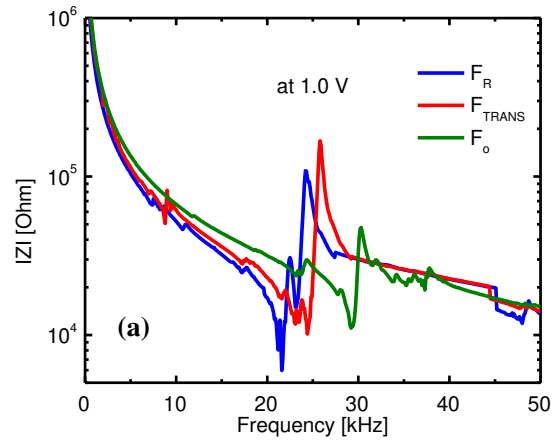


277
278

279 **Figure 4:** Schematic of transducer used in the SPL in-water measurements, explaining crystal
280 placement and application of mechanical bias.

281
282
283
284
285
286
287
288
289
290

291



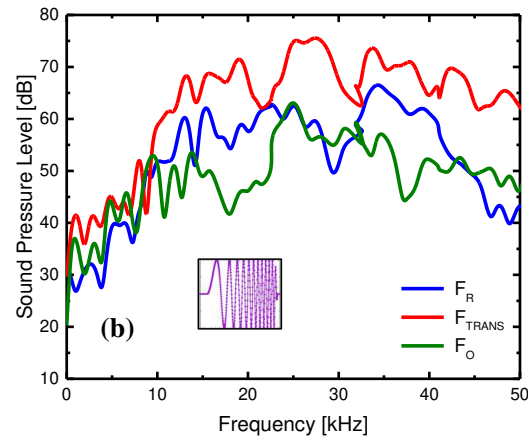
292

293

294 **Figure 5.** (a) Impedance as a function of frequency at 1 V drive. (b) Sound pressure level for three
 295 regimes (F_R , F_{TRANS} , and F_O) in water at 500V drive , normalized to 1m. The inset shows the
 296 formed 1- 40 kHz pulse used for excitation.

297

298



References

- 299 ¹ J. Kuwata, K. Uchino, and S. Nomura, Phase transitions in the Pb (Zn 1/3 Nb 2/3)O 3 -PbTiO
- 300 3 system Ferroelectrics **37**, 579 (1981).
- 301 ² J. Kuwata, K. Uchino, and S. Nomura, Dielectric and Piezoelectric Properties of 0.91Pb(Zn 1/3
- 302 Nb 2/3)O 3 -0.09PbTiO 3 Single Crystals Jpn. J. Appl. Phys. **21**, 1298 (1982).
- 303 ³ J.F. Tressler, T.R. Howarth, and D. Huang, A comparison of the underwater acoustic
- 304 performance of single crystal versus piezoelectric ceramic-based “cymbal” projectors J. Acoust.
- 305 Soc. Am. **119**, 879 (2006).
- 306 ⁴ J.L. Butler and C.H. Sherman, *Transducers and Arrays for Underwater Sound* (Springer
- 307 International Publishing, Cham, 2016).
- 308 ⁵ L.C. Lim, J. Jin, and K.K. Rajan, PZN-PT single crystal underwater devices Proc. US Navy
- 309 Work. Acoust. Transduct. Mater. Devices (2008).
- 310 ⁶ Q. Wan, C. Chen, and Y.P. Shen, Effects of stress and electric field on the electromechanical
- 311 properties of Pb(Mg1/3Nb2/3)O3–0.32PbTiO3 single crystals J. Appl. Phys. **98**, 024103 (2005).
- 312 ⁷ S.-E. Park and T.R. Shrout, Ultrahigh strain and piezoelectric behavior in relaxor based
- 313 ferroelectric single crystals J. Appl. Phys. **82**, 1804 (1997).
- 314 ⁸ E. McLaughlin, T.Q. Liu, and C.S. Lynch, Relaxor ferroelectric PMN-32%PT crystals under
- 315 stress and electric field loading: I-32 mode measurements Acta Mater. **52**, 3849 (2004).
- 316 ⁹ Y. Uesu, M. Matsuda, Y. Yamada, K. Fujishiro, D.E. Cox, B. Noheda, and G. Shirane,
- 317 Symmetry of High-Piezoelectric Pb-Based Complex Perovskites at the Morphotropic Phase
- 318 Boundary: I. Neutron Diffraction Study on Pb(Zn 1/3 Nb 2/3)O 3 –9%PbTiO 3 J. Phys. Soc.
- 319 Japan **71**, 960 (2002).
- 320 ¹⁰ A. Amin, E. McLaughlin, H. Robinson, and L. Ewart, Mechanical and thermal transitions in
- 321 morphotropic PZN-PT and PMN-PT single crystals and their implication for sound projectors
- 322 IEEE Trans. Ultrason. Ferroelectr. Freq. Control **54**, 1090 (2007).
- 323 ¹¹ C. Okawara and A. Amin, dc field effect on stability of piezoelectric PZN-0.06PT single
- 324 crystals under compressive stress Appl. Phys. Lett. **95**, 072902 (2009).
- 325 ¹² M. Davis, D. Damjanovic, and N. Setter, Electric-field-, temperature-, and stress-induced
- 326 phase transitions in relaxor ferroelectric single crystals Phys. Rev. B **73**, 014115 (2006).
- 327 ¹³ A. Amin and L.E. Cross, Elasticity of high coupling relaxor-ferroelectric lead zinc niobate-
- 328 lead titanate crystals J. Appl. Phys. **98**, 094113 (2005).
- 329

This is the author's peer reviewed, accepted manuscript. However, the online version of record will be different from this version once it has been copyedited and typeset.

PLEASE CITE THIS ARTICLE AS DOI: 10.1063/5.0007820

- 330 ¹⁴ P. Finkel, H. Robinson, J. Stace, and A. Amin, Study of phase transitions in ternary lead
331 indium niobate-lead magnesium niobate-lead titanate relaxor ferroelectric morphotropic single
332 crystals Appl. Phys. Lett. **97**, 122903 (2010).
- 333 ¹⁵ P. Finkel, K. Benjamin, and A. Amin, Large strain transduction utilizing phase transition in
334 relaxor-ferroelectric Pb(In₁/2Nb₁/2)O₃-Pb(Mg₁/3Nb₂/3)O₃-PbTiO₃ single crystals Appl.
335 Phys. Lett. **98**, 192902 (2011).
- 336 ¹⁶ P. Finkel, A. Amin, and K. Benjamin, US Patent 8,604,676 (2013).
- 337 ¹⁷ S. Young, M. Staruch, E.A. Patterson, A.N. Caruso, S.E. Lofland, and P. Finkel, Thermally
338 induced phase switching in mechanically biased single crystal relaxors Appl. Phys. Lett. **115**,
339 252901 (2019).
- 340 ¹⁸ C. Vecchini, P. Thompson, M. Stewart, A. Muniz-Piniella, S. R. C. McMitchell, J.
341 Wooldridge, S. Lepadatu, L. Bouchenoire, S. Brown, D. Wermeille, O. Bikondoa, C. A. Lucas,
342 T. P. A. Hase, M. Lesourd, D. Dontsov, and M. G. Cain, "Simultaneous dynamic electrical and
343 structural measurements of functional materials," *Rev. Sci. Instrum.*, vol. 86, no. 10, pp. 103901-
344 10, Oct. 2015.
- 345 ¹⁹ P.-E. Janolin, B. Dkhil, M. Davis, D. Damjanovic, and N. Setter, Uniaxial-stress induced
346 phase transitions in [001]C-poled 0.955Pb(Zn₁/3Nb₂/3)O₃-0.045PbTiO₃ Appl. Phys. Lett. **90**,
347 152907 (2007).
- 348 ²⁰ A.F. Barzegar, D. Damjanovic, and N. Setter, The effect of boundary conditions and sample
349 aspect ratio on apparent d_{33} /piezoelectric coefficient determined by direct quasistatic
350 method IEEE Trans. Ultrason. Ferroelectr. Freq. Control **51**, 262 (2004).
- 351
- 352

This is the author's peer reviewed, accepted manuscript. However, the online version of record will be different from this version once it has been copyedited and typeset.

PLEASE CITE THIS ARTICLE AS DOI: 10.1063/5.0007820

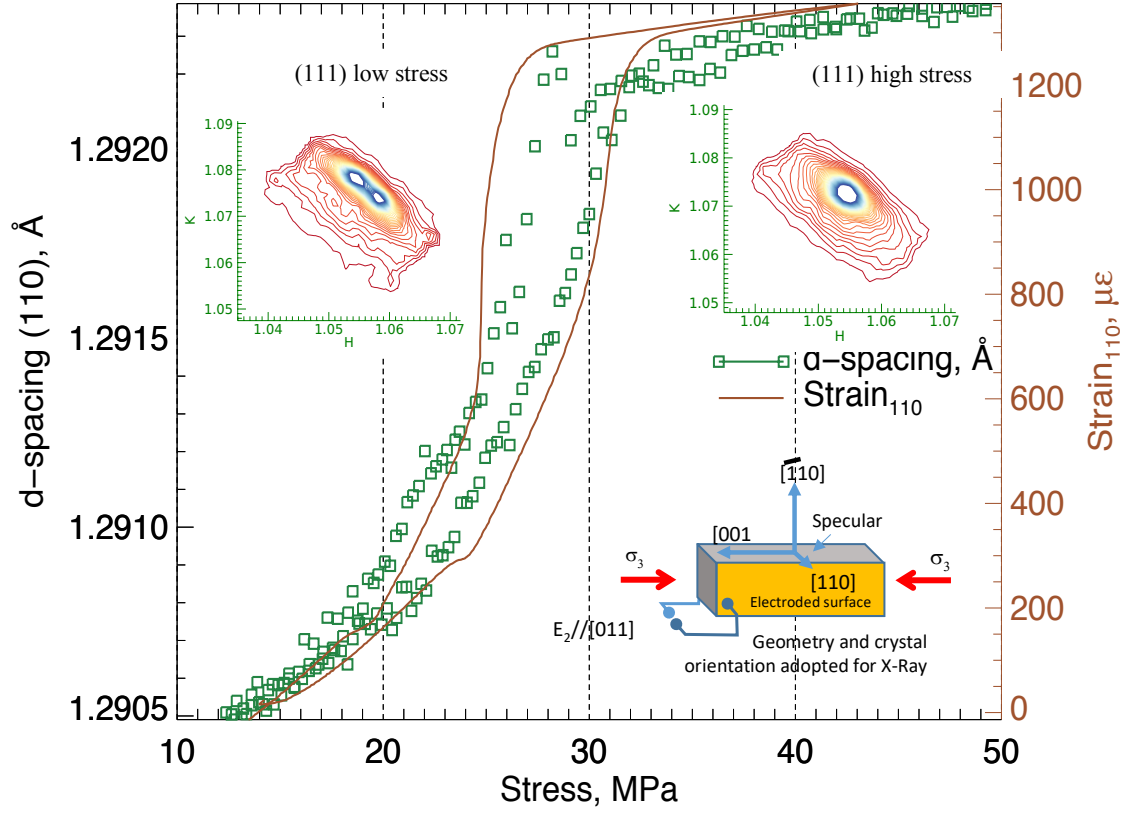


Figure 1

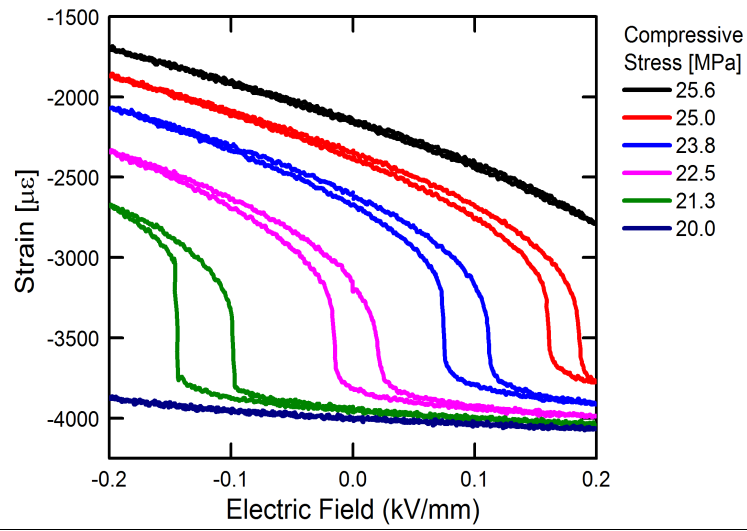


Figure 2

This is the author's peer reviewed, accepted manuscript. However, the online version of record will be different from this version once it has been copyedited and typeset.

PLEASE CITE THIS ARTICLE AS DOI: 10.1063/5.0007820

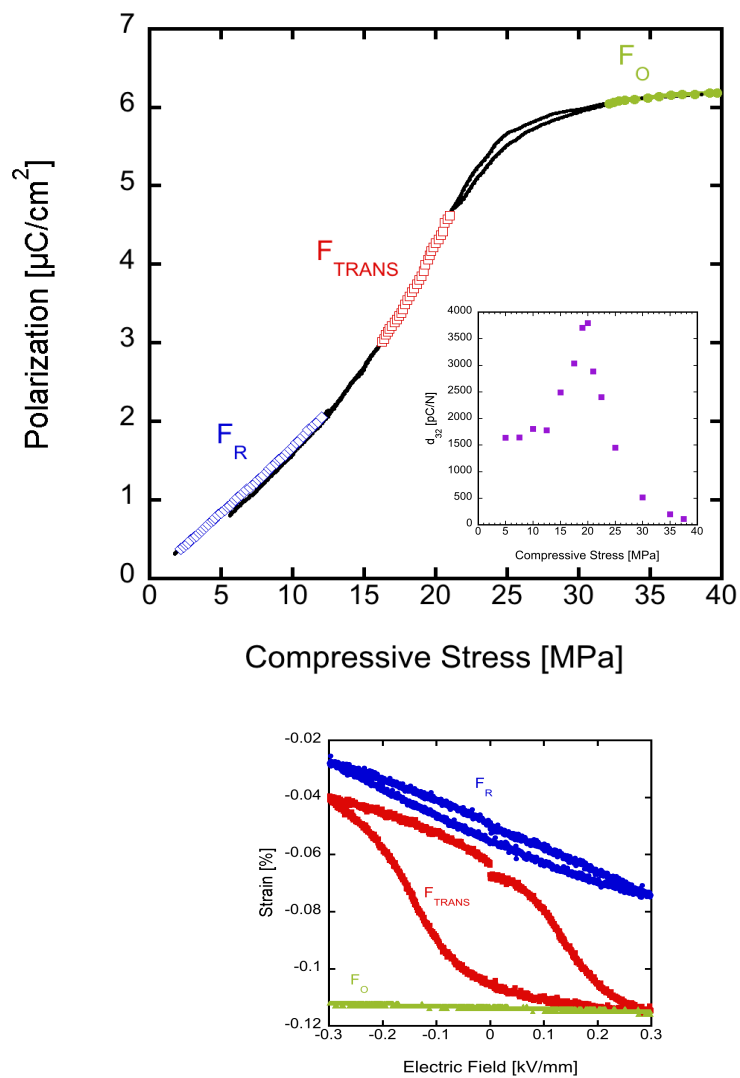


Figure 3.

This is the author's peer reviewed, accepted manuscript. However, the online version of record will be different from this version once it has been copyedited and typeset.

PLEASE CITE THIS ARTICLE AS DOI: 10.1063/5.0007820

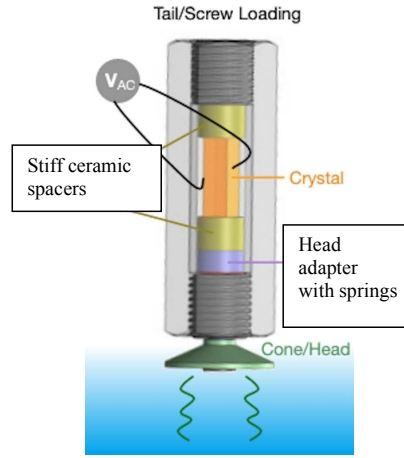


Figure 4:

This is the author's peer reviewed, accepted manuscript. However, the online version of record will be different from this version once it has been copyedited and typeset.

PLEASE CITE THIS ARTICLE AS DOI: 10.1063/5.0007820

1

2

3

4

5

6

7

8

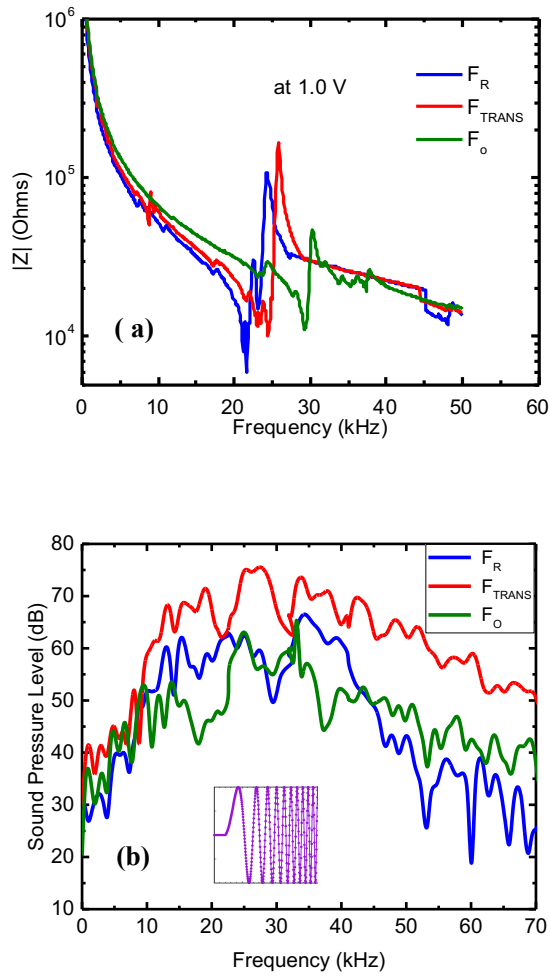


Figure 5.